DC microgrids and battery charging

Maurice Fadel

DC microgrids and battery charging

FADEL Maurice
LAPLACE, Université de Toulouse,
CNRS, INPT, UPS
Toulouse, France
fadel@laplace.univ-tlse.fr
2 rue Charles Camichel,
https://orcid.org/0000-0002-0569-2574

***Abstract*— This paper presents an SAB converter for connecting a DC network to an electric vehicle battery for the purpose of rapid charging. The chosen topology provides galvanic isolation and uses a resonant circuit operating above the resonant frequency. This paper proposes a simple control law to control the battery charging current by acting on the frequency of the resonant circuit using a VCO. The non-linear behavior of the converter is identified by a least squares procedure and the control law is composed of a linear controller and a non-linearity compensation block. Various simulation tests validate the proposal for a wide range of load currents.**

Keywords: Battery charger, SAB converter, Least square method, Power electronics, DC microgrids.

DC grids are multiplying on a large scale and there are more and more features. For electric vehicles, these networks can be combined in an efficient way, especially if we are interested in fast battery charging. Here we present an application that allows a low voltage battery (14v) to be recharged from a more medium voltage source (400v). Fast recharging involves very high currents, so specific converters must be used to ensure good efficiency and flexible adjustment. Many topologies are candidates for this problem but if we seek to increase the efficiency and reduce the volume the solutions based on DAB (Dual Active Bridge) is quickly imposed. Here the function sought being non-reversible we have opted for an SAB (Single Active Bridge) solution. The DAB topology was developed in 1991 [1], [2] and is based on the use of two inverters connected through a high frequency resonant circuit. This topology is characterized by a high efficiency and its reversible character. The output inverter works as a rectifier and it is possible to use only diodes while losing the reversibility to give rise to the SAB. To adapt the output voltage, the resonant circuit can be equipped with a high-frequency transformer, which results in a more efficient solution (Fig. 1). The most commonly used control method for this topology is variable frequency control [3], which consists of varying the impedance of the resonant circuit. Depending on the placement of the switching frequency (fs) relative to the resonant frequency (f0), several conduction modes can be obtained. Two conduction modes can be obtained. These are the continuous (CCM) and discontinuous (DCM) conduction modes. When the switching frequency is higher than the resonance frequency (fs>f0), the current does not perform any half-wave during a half period of operation. Therefore, the diodes are always conductive in the secondary and only the continuous conduction mode can be obtained. The output characteristic is quite particular since it evolves according to the operating frequency. For an operation close to the resonance frequency, it is rather like a voltage source. When we move away from the resonance frequency, it becomes more like a current source (Fig. 2).

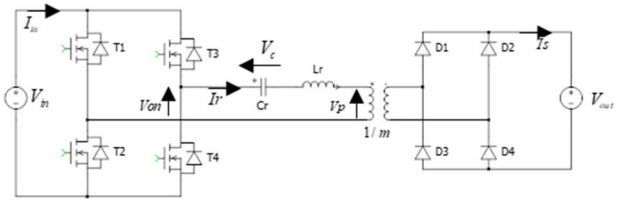

Figure 1: SAB Topology

In a conversion chain, this converter can be seen as an impedance, whose value is related to the reactance of the resonant circuit. Thus for high reactance (fs >> f0), the voltage drop is important. Moreover, a possible short-circuit current at the output of the converter can be limited by increasing the operating frequency. However, the operation with a high ratio between input and output voltages induces a degradation of the power factor in the AC link [4].

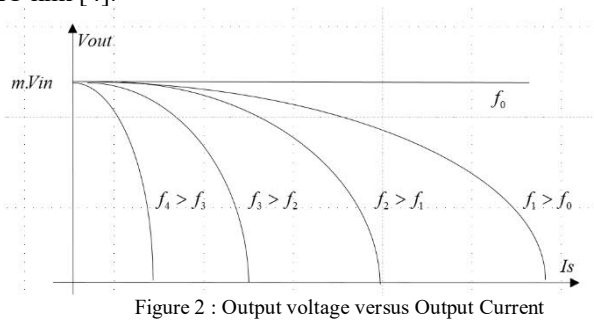

Figure 2 : Output voltage versus Output Current

I. MODELING THE SAB

From Fig. 1 it is easy to see that the voltage Vp is represented by m.Vout where m represents the inverse of the transformation ratio of the transformer. Thus the resonant circuit is located between 2 rectangular voltages Von supplied by the voltage inverter and Vp by the bridge rectifier, (Fig. 3).

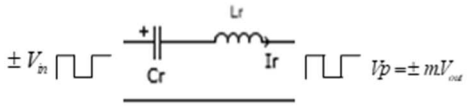

Figure 3: Equivalent Circuit

The switching of the bridge rectifier is natural and depends on the sign of the current in the resonant circuit. From Fig.1 it is easy to see that the voltage Vp is represented by m.Vout where m represents the inverse of the transformation ratio of the transformer. Thus the resonant circuit is located between 2 rectangular voltages Von supplied by the voltage inverter and Vp by the bridge rectifier. The switching of the bridge rectifier is natural and depends on the sign of the current in the resonant circuit. The two source (Von and Vp) are shifted by an angle link to the frequency of solicitation. The evolution of fundamental variables such as the current in the resonant circuit and the average output current can be studied with the following equivalent diagram [5]:

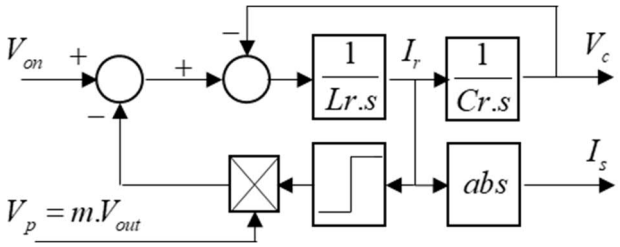

Figure 4: Equivalent bloc diagram

The evolution of the current in the resonant circuit is composed of 4 different segments related to the composition of the voltages +/-Von and +/- Vout, Fig. 5. This characteristic is also visible on the output current, Fig. 6.

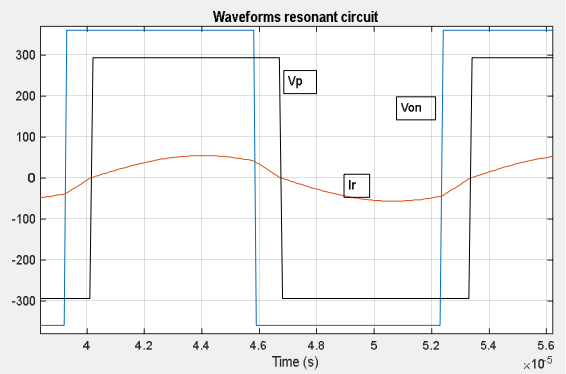

Figure 5: Waveforms resonant circuit for fs=1.2*fo

The amplitude of the current in the resonant circuit depends on the working frequency and the impedance of the circuit at that frequency according to a nonlinear law. When operating above the resonant frequency the average output current will decrease as a function of frequency. Thus the control of this converter can be done by acting on the switching frequency of the inverter. To act continuously on the output current, the use of a VCO is very useful.

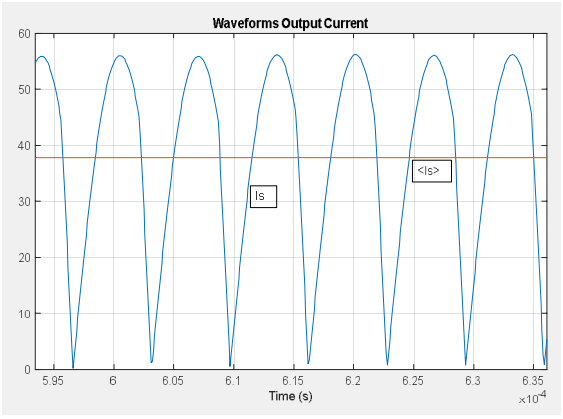

Figure 6: Waveforms Output Current for fs=1.2*fo

1.1 Converter sizing

The converter is sized to provide a maximum charging current of 160 A at 14 V from a high voltage battery with a minimum voltage of 360 V. Thus the parameters are given in Table 1.

TABLE 1. Converter Parameters

Components	Value
Lr	25 µH
Cr	250 nF
Ratio of transformer	m=1/21
Ls	0.1 µH
Cs	960 µF

With the parameters given in table 1 the resonance pulsation is $\omega_0 = \frac{1}{\sqrt{L_r.C_r}} = 4.10^5 rd/s$. The resonance frequency is $f_0 = 63662\ Hz$ and the maximum frequency is set at $f_{s\max} = 3 * f_0$. In per-units $u = f_s / f_0$ the range is from 1 to 3.

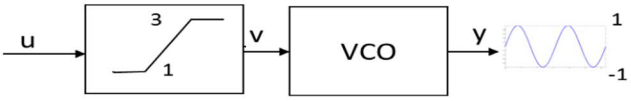

Figure 7: VCO configuration

$$y = \cos(2.\pi.f_0.t + 2.\pi.k_c.\int_0^t v(\tau).d\tau + \varphi) \qquad (1)$$

The parameter k_c represents the sensitivity of the VCO in Hz/V and φ the phase at the origin.

1.2 Output stage with current filtering

To avoid AC currents flowing through the battery it is necessary to filter the output stage with an LC filter sized to attenuate twice the operating frequency of the resonant circuit [6]. Thus we have the following elements:

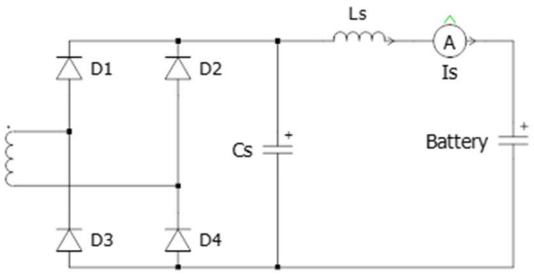

Figure 8: Output Stage with filter

Filtering the output of the inverter is especially important to protect the battery. The frequency of the current is twice the operating frequency and by setting a maximum ripple of e.g. 20%, it is easy to determine the values of the inductance and capacitor, Table 1.

II. IDENTIFICATION OF PARAMETERS CONTROL

For a frequency sweep of u=1.1 to 3 we obtain the following curves Fig. 9, which allows us to construct the following table, Table 2. The simulation is carried out with the PLECS software.

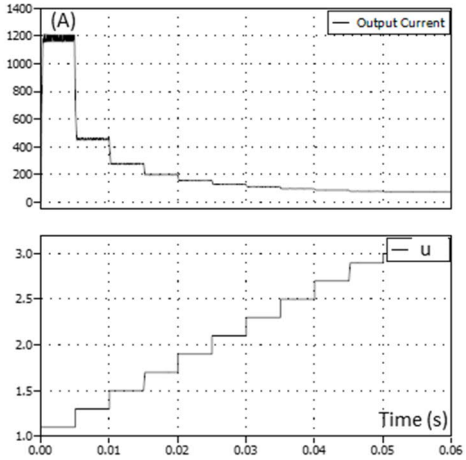

Figure 9: Evolution of output current versus u

TABLE 2. Evolution of output current versus u

Value of u	Average Value of Is (A)
1.1	1185
1.3	458
1.5	279
1.7	201
1.9	158
2.1	132
2.3	113
2.5	99
2.7	88
2.9	80
3	76

Taking into account the resonant circuit model it is easy to show that the relationship between the mean value of the current Is and the reduced frequency u is given by the following relationship:

$$< I_s >= \frac{k.u}{u^2 - 1} \qquad (2)$$

Similarly, the time constant for the average current to build up is approximately constant and the control model can be given by the following diagram:

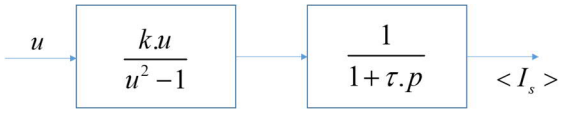

The identification of the constant k can be done by a least squares approach and the constant τ can be deduced from curve 9.

2.1 Identification of gain k

Since the unknown k acts linearly, we can use a least squares method from the measurement table (Table 2).

$$\begin{bmatrix} I_{s1} \\ I_{s2} \\ . \\ . \\ I_{sn} \end{bmatrix} = \begin{bmatrix} \frac{u_1}{u_1^2 - 1} \\ \frac{u_2}{u_2^2 - 1} \\ . \\ . \\ \frac{u_n}{u_n^2 - 1} \end{bmatrix} .k \qquad \text{or vectorially} \quad \underline{Y} = \underline{\Phi}.k \qquad (3)$$

The best approximation of k in the least squares sense is then given by <*k*>:

$$< k >= \left(\underline{\Phi}^t . \underline{\Phi} \right)^{-1} . \underline{\Phi}^t . \underline{Y} \qquad (4)$$

Here $< k > \; = \; 227.31$

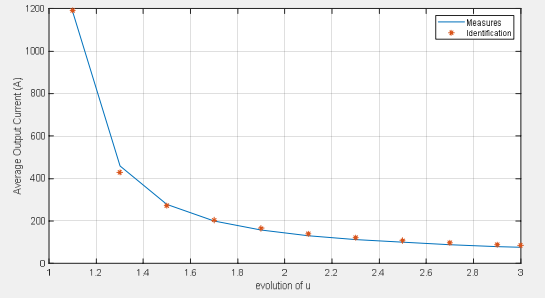

Figure 11. Identification of gain k

2.2 Identification of constant τ

The time constant is essentially constant and an average evaluation can be made graphically by evaluating the time taken for the current to decay by 63% of its initial value.

Thus with several averaged measurements an average value of $\tau = 50\mu s$ is obtained.

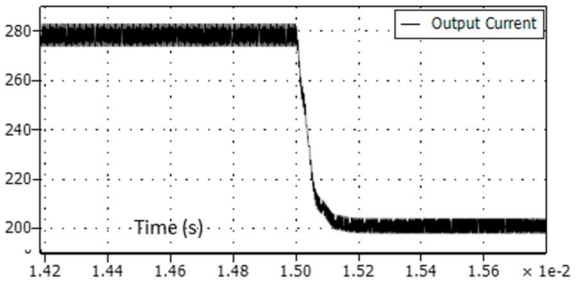

Figure 12: Analyze of time constant

III. INVERTER CONTROL LAW

In order to control the average current in the battery the chosen control law is based on a simple PI regulator and for this it is necessary to linearize the operation of the converter. The linearization is done by model inversion. Indeed, the behavior can be represented by the juxtaposition of a linear block and a non-linear block, Fig. 13. It is therefore necessary to invert the non-linear block by setting up a block representing the reciprocal function $f^{-1}(u)$.

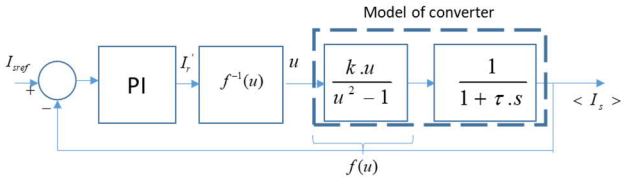

Figure 13: Control law diagram

Thus we get : $u = \dfrac{\sqrt{k^2 + 4.I_r'^2} + k}{2.I_r}$ (5)

Under these conditions, the transfer function seen by the controller can be summarized as:

$$T(s) = \frac{< I_s >}{I_r'} = \frac{1}{1+\tau.s} \quad (6)$$

The evaluation of the average current can be done by a simple filter eliminating twice the operating frequency, in fact we can use a low pass filter set at the frequency of 5 kHz.

3.1 Calculation of the PI controller

For the determination of the parameters several methods can be used (pole placement, symmetric optimum method, ...) [7]. Here we use a simple frequency approach consisting in imposing a bandwidth in closed loop by defining a cut-off pulse of the corrected open loop. The diagram in Fig.14 explains the reasoning behind the asymptotic gain Bode diagram.

It is therefore easy to deduce the parameters of the controller according to the desired bandwidth ω_{bp} determined according to the lowest operating pulsation, i.e. the resonance pulsation ω_0.

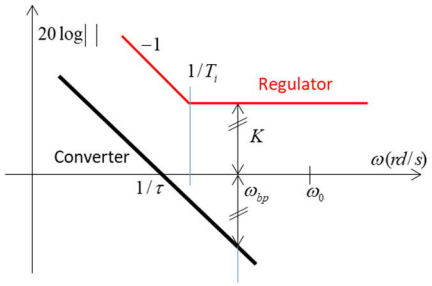

Figure 14: Gain curve of the Bode asymptotic diagram

For a bandwidth of 5000 Hz we obtain the following parameters:

$$\omega_{bp} = 2.\pi.5000 \text{ rd/s} \quad (7)$$

$$K = \tau.\omega_{bp} = 1.57 \text{ and } 1/T_i = \omega_{bp}/\sqrt{10} = 10000 \quad (8)$$

Naturally, in order to achieve correct operation, it is necessary to install an anti-windup as shown in Fig.15 [8].

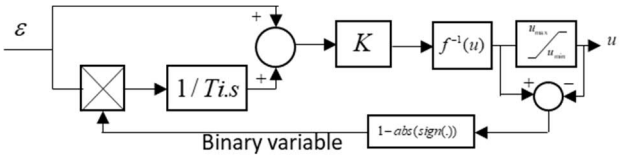

Figure 15: Anti-windup procedure

The principle of this anti-windup is to inhibit the integral action when the control is saturated. This is achieved by means of a multiplier associated with a binary variable.

IV. CLOSED LOOP TESTING

The tests are conducted in simulation using the PLECS software. First, we analyze the variables of the oscillating circuit, i.e. the resonant current and the input and output voltages. Fig. 16 shows this evolution for a current reference of 160 A.

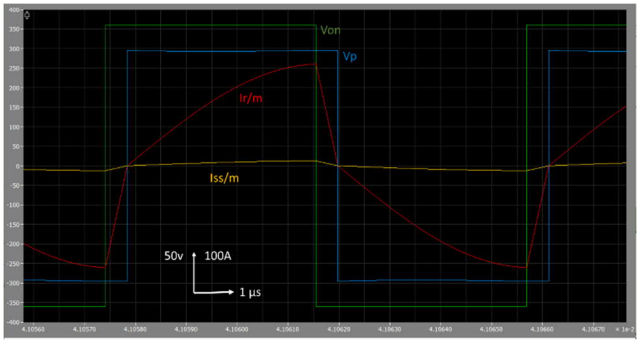

Figure 16: Evolution of resonant circuit variables

The variable I_{ss} represents the current at the secondary of the transformer.

In Fig.17 we can follow the current in the battery and its average value.

Fig.16 and Fig.17 show a controlled operation of the inverter with the charging current installed in the battery as specified.

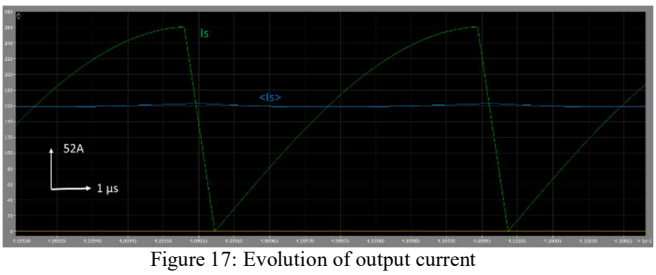

Figure 17: Evolution of output current

We can now look at the transient regime, for example the transition from a reference current of 90A to a reference of 160A, Fig.18 and Fig. 19.

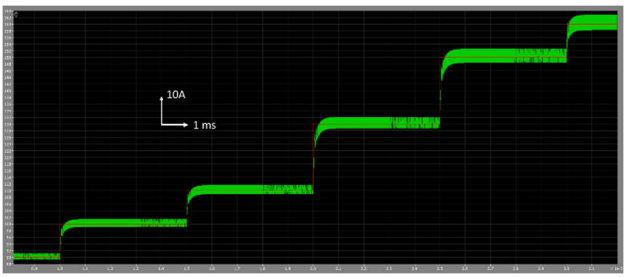

Figure 18: Evolution of the output current at step load from 90 A to 160 A

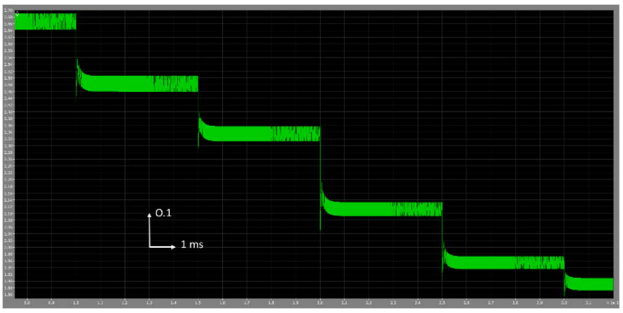

Figure 19: Evolution of the reduced frequency u

These curves show a rigorous control of the operating frequency of the device and the relevance of the linearization by inverse model.

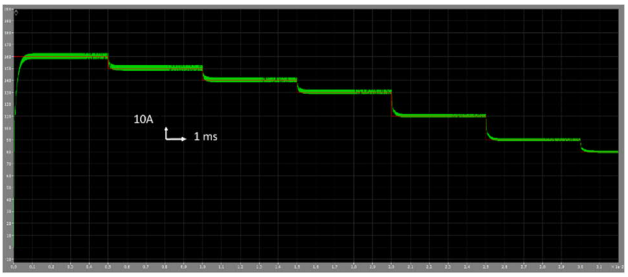

Figure 20: Evolution of the output current at step load from 160 A to 80A

The transformer model here is perfect and assumed to be lossless. Experimental tests will show whether magnetic losses have a significant impact on the behaviour of the converter.
For decreasing changes in the reference current the same behaviour is observed, Fig.20 and Fig. 21.

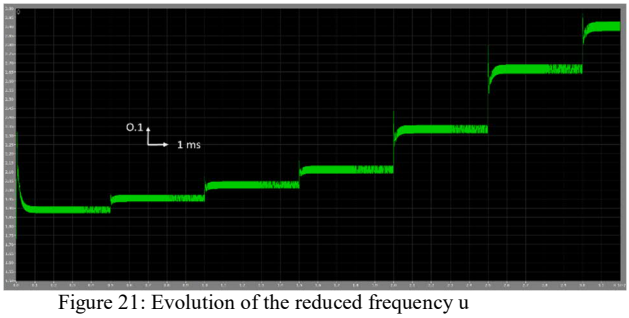

Figure 21: Evolution of the reduced frequency u

V. CONCLUSIONS

In this study, we are interested in the simple control of an SAB-type converter for battery charging from a DC microgrids. The non-linear behaviour of the converter can finally be represented by a non-linear gain associated with a quasi-constant time constant. This model can then be used in a very simple way using a model inversion procedure associated with a PI-type controller. This controller can also be computed very simply using a dedicated frequency approach to impose a closed loop bandwidth.
The simulation results confirm the validity of the approach and the experimental results currently underway will hopefully confirm the validity of the approach.

REFERENCES

[1] R. W. DeDoncker, M. H. Kheraluwala, and D. M. Divan, “Power conversion apparatus for DC/DC conversion using dual active bridges,” United States Patent, Patent Number 5027264, 1991

[2] R. W. A. De Doncker, D. M. Divan, and M. H. Kheraluwala, “A three-phase soft-switched high-power-density DC/DC converter for high-power applications,” Industry Applications, IEEE Transactions on, vol. 27, no. 1, pp. 63–73, Jan. 1991.

[3] R. L. Steigerwald, “High-Frequency Resonant Transistor DC-DC Converters,” IEEE Transactions on Industrial Electronics, vol. IE-31, no. 2, pp. 181–191, May 1984.

[4] M. Marzouk, J.-P. Ferrieux, D. Frey, et B. Sarrazin, “ Considerations to choose an appropriate charger topology for plug-in electric vehicles “, in 2014 16th European Conference on Power Electronics and Applications (EPE’14-ECCE Europe), 2014, p. 1-8.

[5] C. Collomb;M. Fadel;Y. Cheron, “Series resonant converter control: complete tuning of an IP regulator“, Proceedings of IECON'94 - 20th Annual Conference of IEEE Industrial Electronics, 5-9 Sept. 1994, Bologna, Italy

[6] Arzu Turksoya, Ahmet Tekeb Alkan AlkayacA, “Comprehensive overview of the dc-dc converter-based battery charge balancing methods in electric vehicles“, Renewable and Sustainable Energy Reviews, Volume 133, November 2020, https://doi.org/10.1016/j.rser.2020.110274

[7] S. Bacha, A. Hassan, and M. Brunello, “General nonlinear control law for DC-DC symmetric switching converters,” in Power Electronics Specialists Conference, 1993. PESC ’93 Record., 24th Annual IEEE, 1993, pp. 222–228.

[8] K. C. Costa, G. A. Machareth, M. F. Santos, P. Mercorelli, “Classical PI Controllers with Anti-Windup Techniques Applied on Level Systems: An Interesting Case Study“, 2020 International Conference on Mathematics and Computers in Science and Engineering (MACISE).